Chem

CellPress

Article

Seeing Elastin: A Near-Infrared Zwitterionic Fluorescent Probe for *In Vivo* Elastin Imaging

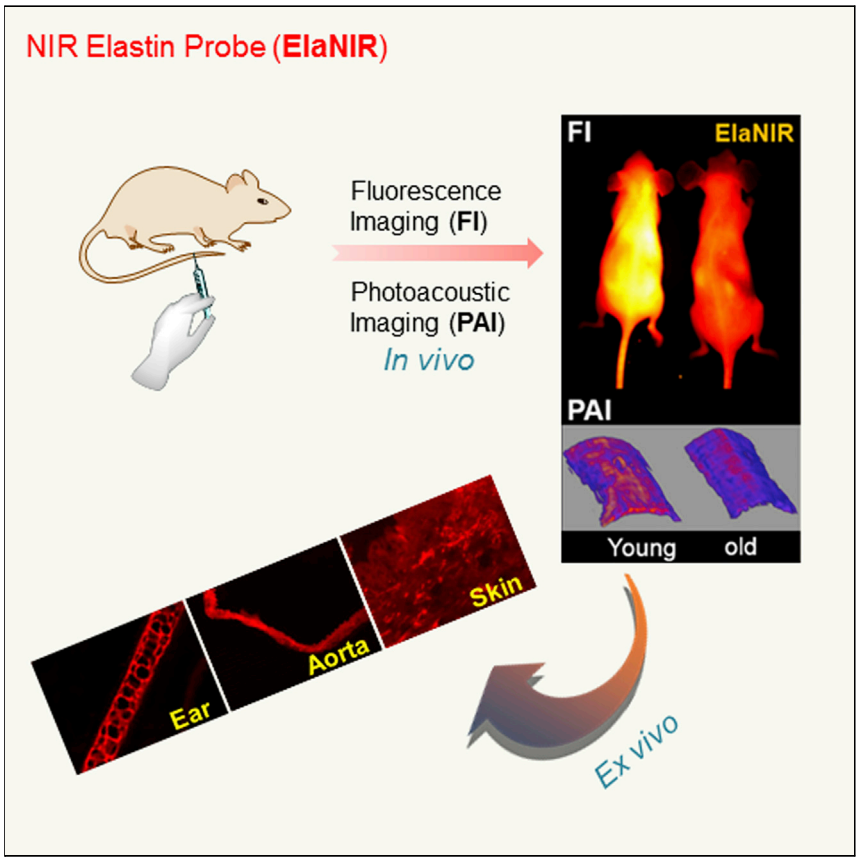

The near-infrared zwitterionic elastin probe **ElaNIR** for *in vivo* imaging of elastin structures was found through fluorescent-image-based screening. **ElaNIR** is well suited for *in vitro*, *ex vivo*, and *in vivo* imaging of elastin and also allows visualization and quantification of elastin levels in young and old mice, which reflect age-dependent changes of elastin *in vivo*.

Dongdong Su, Chai Lean Teoh, Sung-Jin Park, ..., Seong Soon Kim, Myung Ae Bae, Young-Tae Chang

ytchang@postech.ac.kr

HIGHLIGHTS

A zwitterionic NIR fluorophore, **ElaNIR**, was found to selectively bind elastin

ElaNIR is well suited for *in vitro*, *ex vivo*, and *in vivo* imaging of elastin

ElaNIR showed age-dependent changes of skin elastin levels

Su et al., Chem 4, 1128–1138
May 10, 2018
https://doi.org/10.1016/j.chempr.2018.02.016

Chem

CellPress

Article

Seeing Elastin: A Near-Infrared Zwitterionic Fluorescent Probe for *In Vivo* Elastin Imaging

Dongdong Su,[1,9] Chai Lean Teoh,[1,9] Sung-Jin Park,[1] Jong-Jin Kim,[1] Animesh Samanta,[1] Renzhe Bi,[4] U.S. Dinish,[4] Malini Olivo,[4] Marie Piantino,[5] Fiona Louis,[6] Michiya Matsusaki,[5,6,7] Seong Soon Kim,[8] Myung Ae Bae,[8] and Young-Tae Chang[1,2,3,10,*]

SUMMARY

Elastic fibers are present in a variety of tissues and are responsible for their resilience. Until now, no optical contrast agent in the near-infrared (NIR) wavelength range of 700–900 nm has been reported for the imaging of elastic fibers. Here, we report the discovery of a NIR zwitterionic elastin probe ElaNIR (elastin NIR) through fluorescent-image-based screening. The probe was successfully applied for *in vitro*, *ex vivo*, and *in vivo* imaging by various imaging modalities. Age-related elastin differences shown by *in vivo* fluorescent and photoacoustic imaging indicated that ElaNIR can be a potentially convenient tool for uncovering changes of elastin in live models.

INTRODUCTION

Elastin is a key structural protein found in the extracellular matrix (ECM). It is secreted primarily by fibroblast cells, which assemble into fibers and cross-links to form a mechanically flexible network of fibers and sheets.[1] To yield a wide range of structures with tailored elastic properties, the arrangement of elastin in the ECM can vary between tissues. Elastin in the form of lamina in the arterial wall is crucial for the strength necessary for vessel expansion and regulation of blood flow, whereas elastin fibers are enriched in the dermis of the skin to impart flexibility and extensibility.

Different from other connective tissue proteins such as collagens, which are members of large and complex gene families, elastin is encoded only by a single tropoelastin gene (*ELN*). As *ELN* expression is turned down substantially from a young age, we rely mostly on the elastin that was produced before birth and in the first few years of life.[2,3] A low level of elastin production means that any damage cannot be efficiently repaired as tissues gradually lose their elasticity. Visualization of elastin architecture and its dynamic changes in live tissues will therefore provide better understanding about its roles in biological processes.

Despite its high importance, elastin is difficult to image. So far, methods for easy and high-resolution imaging of elastin *in vivo* or *in situ* are limited. Reported methods of studying their morphology have largely been restricted to either exploiting the intrinsic fluorescence properties of elastin or using histologic dyes, which are incompatible with intravital studies. Recently, staining of elastin by fluorescent labeling, such as sulforhodamine B, Col-F, and Alexa Fluor 633, has been reported in selected tissues.[4–6] Further *in vivo* applications, however, are impeded by the probes' short

The Bigger Picture

Technological advancement of microscopic imaging has spurred the development of molecular probes for the detection of biologically and environmentally important analytes. Among fluorescent imaging tools, near-infrared (NIR) fluorescent molecules have been popular for *in vivo* imaging because of their ability to penetrate tissue deeper with reduced scattering and autofluorescence. Here, we report the discovery of the NIR zwitterionic elastin probe ElaNIR. We found that ElaNIR showed selective binding for elastin, such as those in the aorta, lungs, and skin. ElaNIR also allowed visualization and quantification of elastin levels in young and old mice, which reflect age-dependent changes of elastin *in vivo*. This makes ElaNIR a unique chemical tool for monitoring changes of elastin in tissue or animal models and provides new opportunities to study the effects of chemical compounds on elastin levels in biological processes.

emission wavelengths because visible light can penetrate only a few hundred micrometers below the tissue surface. Near-infrared (NIR) light, on the other hand, penetrates millimeters up to centimeters into living tissue and hence holds greater promise over other small molecules.[7–9]

Inspired by the outstanding features of **ZW800-1** in earlier reports,[10–12] we synthesized a zwitterionic NIR library, **CyZW**, by introducing structural diversity to the key structure of **ZW800-1** while retaining its superior chemical and photophysical properties for bioimaging. The diversity-oriented fluorescence library (DOFL) approach has proven its versatility in sensor development, especially during the absence of mechanistic cues to rationally design probes.[13–18] We present dye **CyZW-599** from DOFL screening, also dubbed **ElaNIR** (elastin NIR), as a bioimaging probe for elastin.

RESULTS AND DISCUSSION

Library Design, Characterization, and Optical Properties

The recently developed zwitterionic NIR fluorophore, **ZW800-1** has shown superior *in vivo* properties, including low serum binding, ultra-low non-specific tissue background, and rapid clearance from the body via renal filtration, over other NIR dyes.[10] Despite that, limitations in its structural diversity have hindered **ZW800-1** for potential downstream applications. To overcome this limitation and to expand the application of zwitterionic NIR dyes, we designed a family of dyes based on **ZW800-1**. Firstly, the key intermediate, **ZW800-1**, was successfully synthesized as previously reported.[10] A broad range of structural diversities were then constructed quite efficiently by the reaction of a series of primary amines with *tert*-butyl 2-bromoacetate. Finally, **ZW800-1** was coupled with the diversity amine building blocks by a standard coupling protocol.[19,20] The final step involved de-protection of the acid linker to yield 64 members of the **CyZW** library (Scheme 1 and Figure S1). Each **CyZW** compound contains a single carboxylic acid at the end of the structure, which will be useful for further downstream modifications such as conjugation with various reporter or affinity tags for bio-conjugation depending on the experimental design requirements.

Spectra properties of the newly synthesized library **CyZW** were measured in DMSO. Because all the **CyZW** compounds share the same core structure, they display similar optical properties. **CyZW** compounds show maximum absorption and emission wavelengths at about 790 and 805 nm, respectively, in DMSO. The zwitterionic **CyZW** dyes show a high extinction coefficient of more than 200,000 M^{-1} cm^{-1} and a much higher quantum yield (average of 0.39) than other NIR dyes (Table S1). This is a great improvement because fluorescence intensity is crucial for practical applications, in particular for achieving better-resolution images during *in vivo* imaging.

ElaNIR, a NIR Fluorescent Elastin Probe

Screening of the **CyZW** library revealed compounds with apparent specificity for elastin. When frozen mouse aorta tissues were treated with **CyZW** dye solution, we observed cases where a network of fibers were readily stained and became highly visible under the fluorescence microscope (Figure 1A). These were identified to be elastin fibers. The medial lamellar unit of the aorta wall is constructed with elastin arranged in concentric lamellae and smooth muscle cells that lie in between.[21,22] After evaluating the screened library for its fluorescence intensity and selectivity, we selected **ElaNIR** (**CyZW-599**) as the best compound for further studies (Figures S2 and S3) and selected **CyZW-274**, which ranked low in the image-based scoring,

[1]Laboratory of Bioimaging Probe Development, Singapore Bioimaging Consortium, Agency for Science, Technology, and Research (A*STAR), 11 Biopolis Way, 02-02 Helios, Biopolis, Singapore 138667, Singapore

[2]Centre for Self-assembly and Complexity, Institute for Basic Science, Pohang 37673, Republic of Korea

[3]Department of Chemistry, Pohang University of Science and Technology, 77 Cheongam-Ro, Nam-Gu, Pohang 37673, Republic of Korea

[4]Bio-optical Imaging group, Singapore Bioimaging Consortium, Agency for Science, Technology, and Research (A*STAR), 11 Biopolis Way, 02-02 Helios, Biopolis, Singapore 138667, Singapore

[5]Department of Applied Chemistry, Graduate School of Engineering, Osaka University, 2-1 Yamadaoka, Suita, Osaka 565-0871, Japan

[6]Joint Research Laboratory (TOPPAN) for Advanced Cell Regulatory Chemistry, Graduate School of Engineering, Osaka University, 2-1 Yamadaoka, Suita, Osaka 565-0871, Japan

[7]JST, PRESTO, 4-1-8 Honcho, Kawaguchi, Saitama 332-0012, Japan

[8]Bio&Drug Discovery Division, Korea Research Institute of Chemical Technology, Yuseong-Gu, Gajeongro 141, Daejeon 34114, Republic of Korea

[9]These authors contributed equally

[10]Lead Contact

*Correspondence: ytchang@postech.ac.kr

https://doi.org/10.1016/j.chempr.2018.02.016

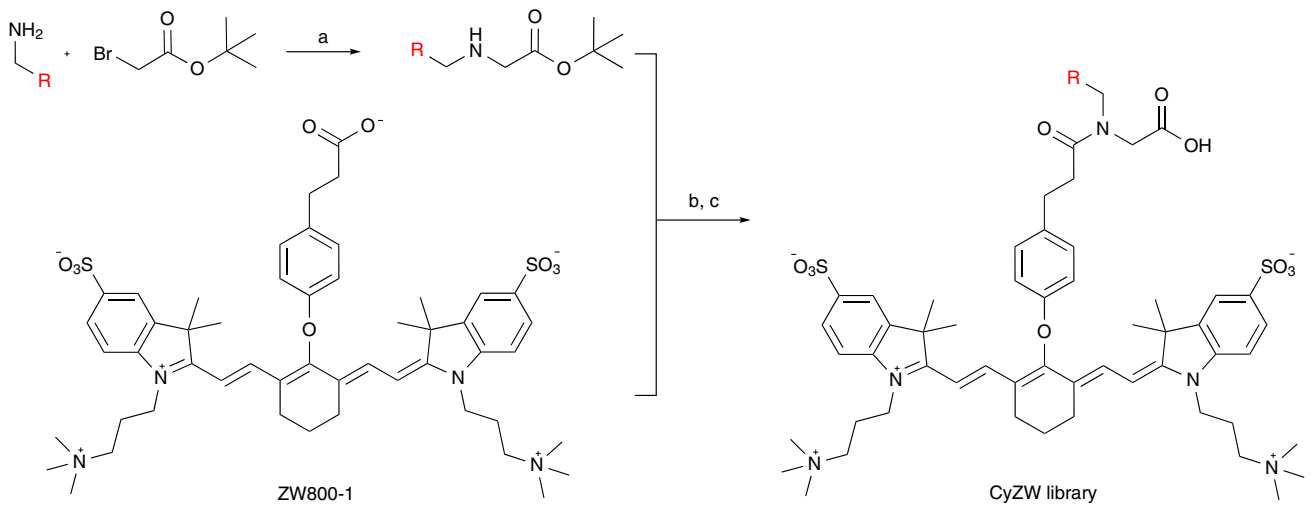

Scheme 1. Synthetic Scheme for the CyZW Library

Reagents and conditions: (a) 64 different aromatic and aliphatic primary amines, acetonitrile, *N*,*N*-diisopropylethylamine (DIEA), room temperature (RT), 2 hr; (b) DMSO/DMF (1:4), HATU, DIEA, RT, 3 hr; (c) 20% trifluoroacetic acid in dichloromethane, RT, 3 hr. See also Figure S1.

as a negative control compound (Figure S4). On the other hand, when spectroscopy-based screening was conducted, the *in vitro* screening results were unable to distinguish elastin specificity of different dyes within the library. There could be no change in the structure and motion of the dye before and after analyte is added, resulting in a small or no change in its fluorescence intensity or anisotropy. Thus, we found the *in vitro* detection of elastin protein in solution by spectroscopy methods unsuitable; the tissue-based screening approach was better suited for distinguishing an elastin-selective probe. Optical properties of **ElaNIR** and **CyZW-274** in different solvent systems are detailed in Figure S5 and Table S2. Both dyes showed more fluorescence in the presence of warm serum than PBS alone. Optical parameters for both dyes are similar in the same solvent system.

Elastin is a very non-polar protein, often with no negatively charged amino acids, and most of the positively charged amino acids are lost when the lysines form cross-links that convert the soluble monomer, tropoelastin, to insoluble, polymeric elastin in tissues. Although it is still unclear, some elastin-staining dyes can be based on hydrophobic interactions that take place with many sites along the elastin molecule.[23] We evaluated the distribution coefficient (log*D*) of the **CyZW** library at pH 7.4, which is an important parameter for evaluating the hydrophobicity of a compound. At pH 7.4, log*D* values varied from −5.12 (**CyZW-414**) to 2.94 (**CyZW-656**) (Table S1). Comparison of the log*D* data with scoring from fluorescence image-based screening (Figure S6) showed that log*D* alone is not a predictive measure of elastin specificity fate. Nonetheless, some correlation existed near a log*D* value of 0, which implies that the majority of compounds that fell on either side, with more negative or positive log*D* values, might not have enough affinity for elastin or might have high background signal toward neighboring tissues.

NMR and molecular dynamics data on elastin in both the monomeric and polymeric states all support the conformational flexibility of elastin.[24] There is no single structure for elastin; rather, the protein is made up of an ensemble of rapidly interconverting conformations. Thus, it is not possible to designate a simple "structural model," which makes deducing a binding mechanism of **ElaNIR** for elastin especially challenging. On the basis of the structural-activity relationship observations

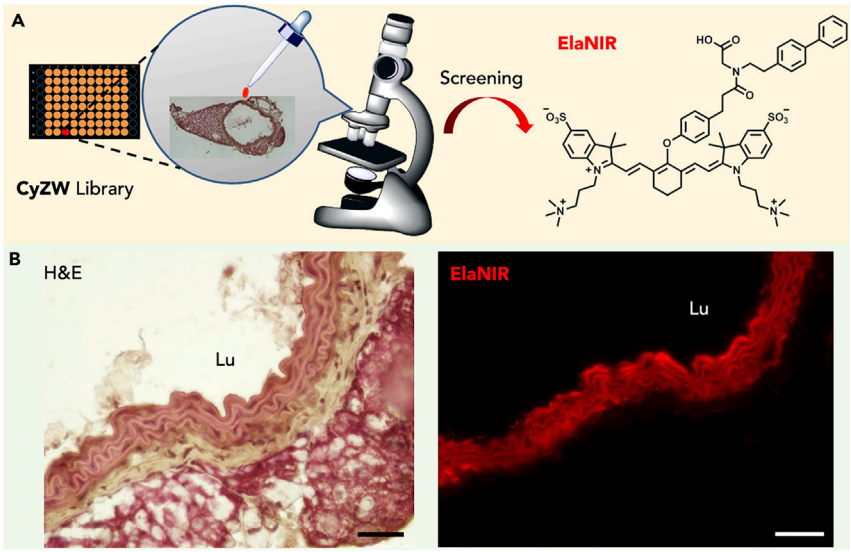

Figure 1. ElaNIR, an NIR Fluorescent Elastin Probe

(A) Discovery of **ElaNIR** by image-based screening and its chemical structure.

(B) **ElaNIR** *ex vivo* staining of elastin lamellae. H&E staining of the aorta (left) and **ElaNIR** staining of elastin (right) are shown. Scale bars, 50 μm. Lu, lumen.

See also Figures S2, S4, and S7.

from our screening results, we postulate that the biphenyl group in **ElaNIR** could play a role in elastin specificity because the absence of the biphenyl structure diminished the elastin selectivity of the other fluorophores within the **CyZW** library. This is only speculative given that the precise molecular target for binding is not yet known.

ElaNIR Enables *Ex Vivo* Detection of Elastin

As a preliminary bioimaging test for **ElaNIR**, the dye was administered intravenously (i.v.) into mice, and **CyZW-274**-injected and non-injected animals were used as controls. One hour after the compound was administered, the animals were sacrificed, the organs were harvested, and cryosections were prepared for analysis. Figure 1B shows H&E staining of the aorta cross-section. A strong NIR fluorescence signal was observed in **ElaNIR**-injected mice, which showed clear staining of the elastic lamellae (Figure 1B). In contrast, there was no detectable NIR signal in **CyZW-274**-injected mice and non-injected control mice (Figure S7), reinforcing the notion that **ElaNIR** exhibits affinity for elastin structures.

To confirm the observation separately by immunohistochemical staining with elastin antibody, we prepared cryosections from organs with high-elastin content, such as the lungs, skin, and bladder, in addition to the kidneys, aorta, and ears (Figures 2 and S8). An **ElaNIR** signal was captured, and consecutive sections were fixed in paraformaldehyde for immunohistochemistry (IHC). Figure 2A shows abundant **ElaNIR**-stained elastic fibers in the lungs, and fine, wispy elastic structures were detected by **ElaNIR** in the skin dermis (Figure 2B). The urinary bladder also showed the highly elastic urothelium brightly stained by **ElaNIR** (Figure 2C). In addition, the kidney revealed an **ElaNIR** signal in the renal artery or vein, as well as calyx, without much noticeable signal in other regions (Figure S8). Both aorta and ear tissue sections stained by **ElaNIR** gave clear strong signals consistent with antibody staining (Figure S8). On the other hand, IHC was also performed on selected tissues with

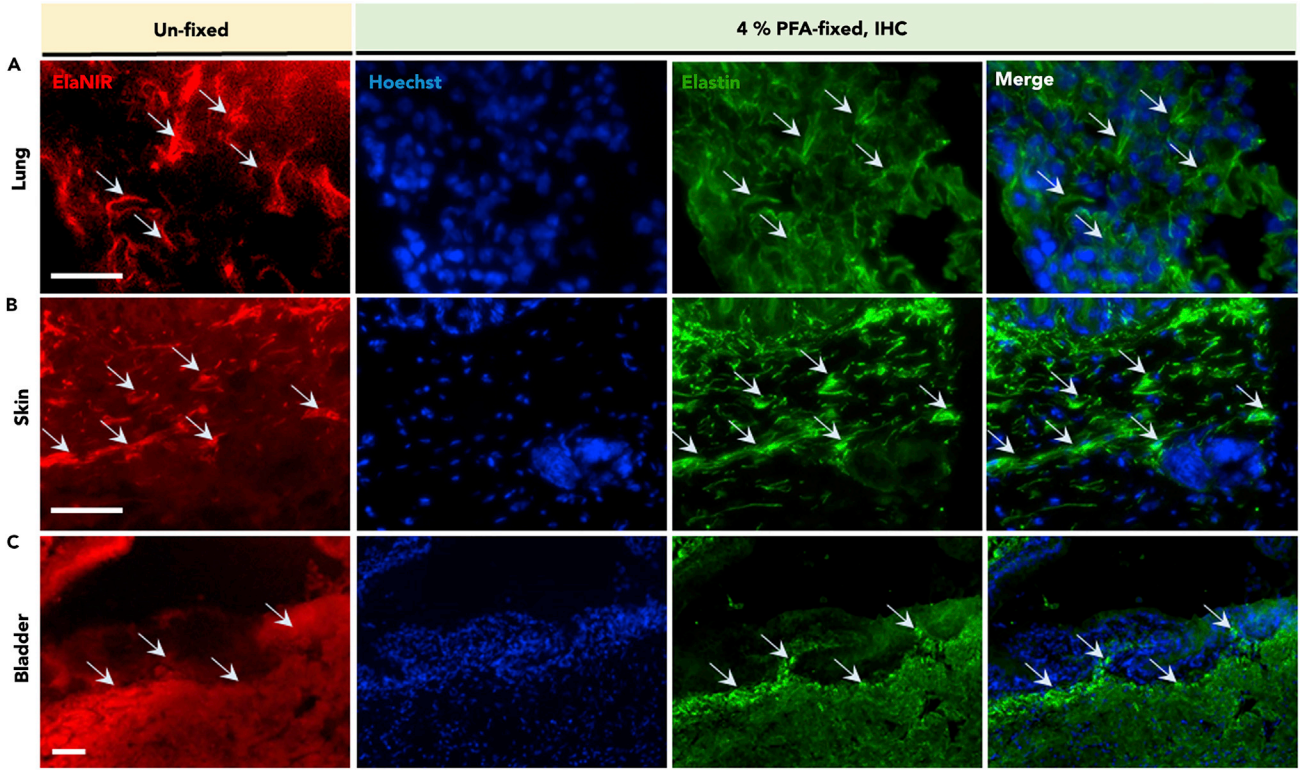

Figure 2. ElaNIR Enables *Ex Vivo* Detection of Elastin

Cryosections were prepared from organs including the lungs (A), skin (B), and urinary bladder (C). **ElaNIR** signal was detected in the NIR channel (left panels). Consecutive sections were fixed with 4% paraformaldehyde, and IHC was performed with an anti-elastin antibody co-stained with Hoechst. Merged images are shown in the right panels. White arrows show elastin fibers. Scale bars, 100 μm. See also Figures S8 and S9.

anti-collagen antibody, which is another major ECM component, and was found to be inconsistent with signals displayed by **ElaNIR** (Figure S9). Cryosections prepared from organs of a **CyZW-274**-injected mouse showed negligible signal (Figure S10).

Elastin Detection in 3D Tissue Models

Elastin, a major component of the ECM, is a crucial but often overlooked element in tissue regeneration. We applied **ElaNIR** to directly visualize the production of elastin fibers in a 3D tissue model, where human umbilical artery smooth muscle cells (UASMCs) were seeded in a suspension of collagen microfibers, leading to ball tissues. Figure 3A shows a small amount of fibers externalized by UASMC ball tissues after 3 weeks in culture. Despite the presence of another major extracellular protein component, i.e., collagen, preferential staining of elastin fibers by **ElaNIR** further supported its selectivity (Figure S11). As shown in Figure 3B, **ElaNIR** staining of extracellular elastin fibers within the collagen mass is consistent with elastin antibody staining. We envisage that when **ElaNIR** is combined with a 3D tissue model system, it has the potential to serve as a powerful platform for assessing the potency of compounds targeted at increasing elasticity.

In Vivo Elastin Targeting with ElaNIR

The observations so far give us strong confidence that **ElaNIR** could be further explored for *in vivo* imaging. The pharmacokinetics of **ElaNIR** was studied by quantification of the dye in blood plasma over several time points during a 24-hr

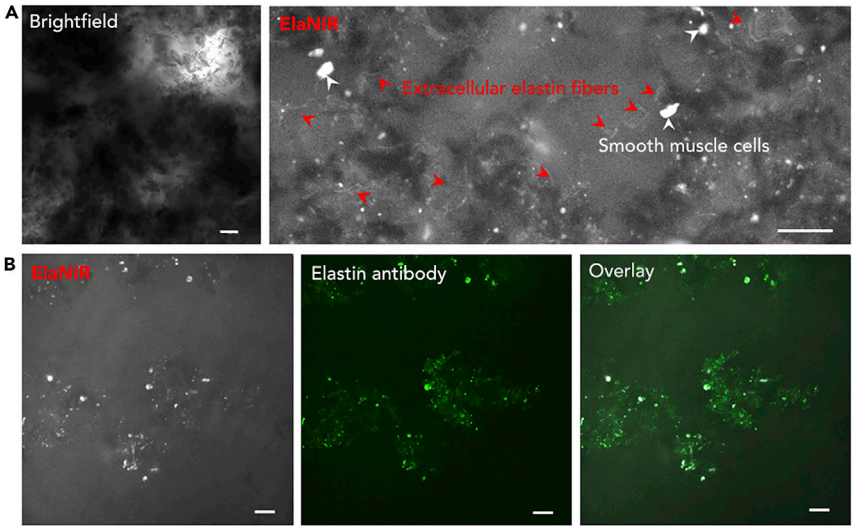

Figure 3. Elastin Detection in 3D Tissue Models

(A) Bright-field signal (left) and **ElaNIR** signal in the NIR channel (right).

(B) **ElaNIR** signal detected in the NIR channel (left), signal from an anti-elastin antibody (middle), and overlay imaging (right).

Scale bars, 100 μm. See also Figure S11.

period (Table S3 and Figure S12). More than 90% of the injected dose (ID) was eliminated from the plasma shortly after 4 hr (0.087 ± 0.032 %ID/g), a decrease from 6.30 ± 0.60 %ID/g at 0.083 hr after intravenous injection. At 24 hr, only 0.0040 ± 0.0017 %ID/g dye remained in the plasma. At 4 hr after injection, organs were also resected and dye distribution measured. The most intense uptake for **ElaNIR** was measured primarily in the kidneys (5.01 ± 2.14 %ID/g), consistent with active renal excretion (Tables S4–S6). For *in vivo* visualization, a nude mouse received an i.v. injection of **ElaNIR**, and the fluorescence signal was monitored by an IVIS Spectrum imaging system. Figures 4A and 4B show a robust fluorescence signal from the whole body of the mouse injected with **ElaNIR**, and intense signal came from the urinary bladder (Figure S13). On the other hand, a diminished fluorescence signal was observed in a mouse injected with **CyZW-274**, and a non-injected control mouse did not show any signal (Figure S14).

At the end of *in vivo* monitoring, the **ElaNIR**-injected animal was sacrificed and observed *ex vivo* on the same imaging system. A fluorescence signal was no longer observed at the head region after the skin was removed to reveal the skull. This indicates that the fluorescence signal does not originate from the organ beneath the skin. Instead, a strong signal was observed from the skin and the base of the ear, both of which are rich in elastic structures. Also, by removing the organs from the chest and abdominal cavity, we observed clear staining in the intact major blood vessel joining the heart to the kidney (Figure 4C). Comparison of the fluorescence distribution in the various vital organs showed that the lungs and kidneys gave strong signals (Figure 4D). This is unsurprising because the lungs are richer in elastin than the other vital organs observed, whereas the kidneys are highly vascularized. We also expect an **ElaNIR** signal from the urinary bladder because it is an elastic organ, consistent with the immunohistochemical observations. In addition, the zwitterionic NIR compound was excreted primarily through the renal clearance pathway, which could also have contributed to the signals observed in renal organs.

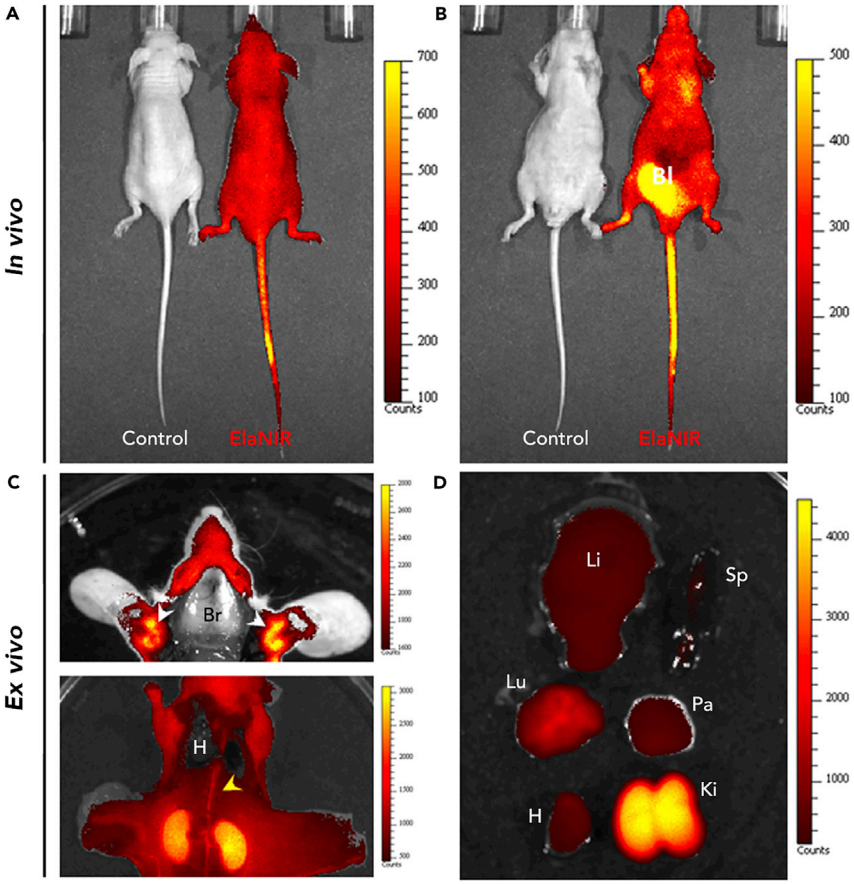

Figure 4. *In Vivo* Elastin Targeting with ElaNIR

(A and B) Dorsal (A) and ventral (B) images of nude mice were captured *in vivo* on the IVIS Spectrum imaging system 60 min after i.v. injection with **ElaNIR**. Non-injected mice were used as controls. (C and D) Animals were sacrificed at the end of observation and imaged *ex vivo*. (C) **ElaNIR** staining of elastic cartilage at the base of the ears (white arrow; top), in the aorta (yellow arrow), and in the kidneys (bottom). (D) The distribution of **ElaNIR** in vital organs. Bl, bladder; Br, brain; H, heart; Ki, kidney; Li, liver; Lu, lung; Pa, pancreas; Sp, spleen.

See also Figures S13 and S14.

ElaNIR Shows Differences between Young and Old Skin

Encouraged by the *in vivo* observations, we further explored the applicability of **ElaNIR** by using a set of spectroscopic and optical imaging experiments performed on young and old mice (1 and 10 months old, respectively).

Diffuse reflectance spectroscopy (DRS) provides a versatile platform for tissue characterization because it is primarily dependent on tissue optical parameters. Because of the strong light absorption of endogenous absorbers in the visible NIR region, DRS offers great value for the classification and analysis of tissue samples.[25] Figure S15A shows a difference in the DRS spectra between young and old mice before **ElaNIR** injection. The relatively higher reflectance signal from the young mouse can be explained by the presence of endogenous absorbers in the skin.

After **ElaNIR** injection, a dip observed in the spectra at ~780 nm indicates the presence of the probe in the skin (Figure S15B). Lower reflectance from the skin of the younger mouse indicates higher absorption of light, which in turn implies greater content of

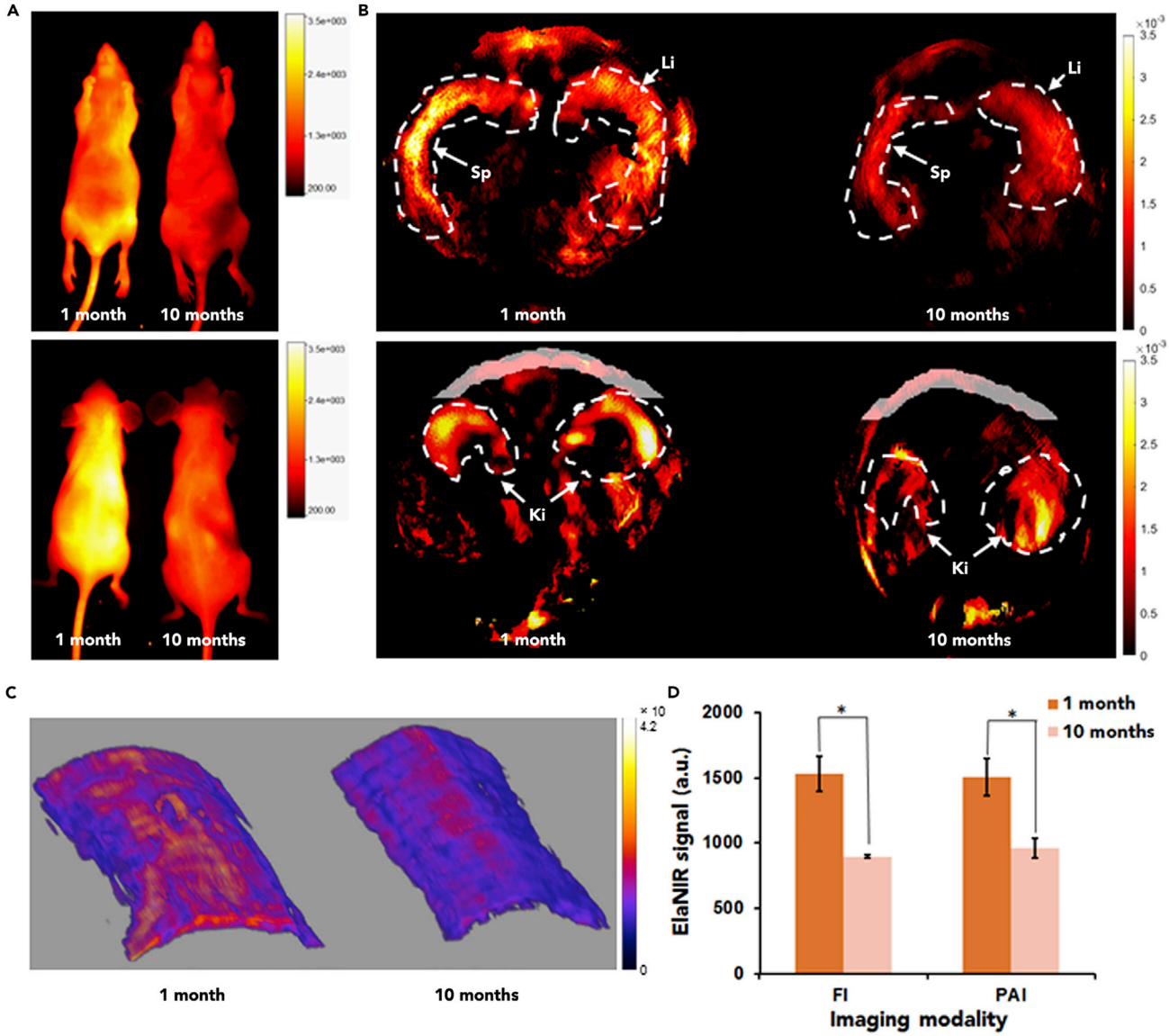

Figure 5. ElaNIR Shows Differences between Young and Old Skin

(A) Ventral and dorsal images of 1-month-old and 10-month-old nude mice were captured *in vivo* on the In-Vivo Xtreme imaging system 1 min after i.v. injection with **ElaNIR**. Non-injected mice were used as controls (not shown).

(B) Selected photoacoustic images of 1-month-old and 10-month-old nude mice were captured *in vivo*. The highlighted areas in the bottom panel show the selected ROIs presented in (C). Ki, kidney; Li, liver; Sp, spleen.

(C) Reconstructed skin images for 1-month-old and 10-month-old mice from the selected ROIs of transverse slices in (B).

(D) **ElaNIR** signal for 1-month-old and 10-month-old mice by both imaging modalities. Data are represented as mean ± SD; *p < 0.05.

See also Figures S15 and S16.

elastin in the skin. It was also noticed that the spectral profile is dominated by the signal from **ElaNIR** after injection, which masks the contribution of endogenous markers in the 650–850 nm range. Because DRS is a point measurement, the difference in the reflectance intensity value cannot be explicitly used for quantitative evaluation. However, it can be used a fast approach to confirm the presence of the probe in the skin.

An **ElaNIR** fluorescence signal was first monitored by In-vivo Xtreme before injection and immediately after the probe was injected (Figure 5A). We observed higher

ElaNIR fluorescence signals from 1-month-old mice than from 10-month-old animals. The mean of three sets of imaging experiments (dorsal and ventral combined) gives a fold change of ~1.68. In addition, photoacoustic imaging (PAI) was also used for the relative quantification of **ElaNIR** targeting elastin in the skin of young and old mice. PAI has recently emerged as an exciting imaging modality because of its unique advantage in providing functional, anatomic, and molecular information at microscopic resolution at a higher imaging depth than other existing modalities.[26–28] In PAI, samples are irradiated with short laser pulses, which are absorbed by endogenous (e.g., hemoglobin and melanin) or exogenous contrast agents, leading to a rapid and transient increase in temperature (in the order of mK) and resulting in thermo-elastic expansion. These optically non-scattering acoustic waves can be detected by ultrasound transducers. The acoustic data can then be used to reconstruct 2D or 3D optical absorption maps with a high spatial resolution (<100 μm) and a penetration depth up to a few centimeters. Hence, PAI exploits the advantage of an optical technique in terms of molecular specificity and resolution along with that of high-frequency ultrasound for deep-tissue interrogation.[28–30]

In order to distinguish photoacoustic (PA) signal by **ElaNIR** in the skin area, we selected a small region of interest (ROI) near the spine region (Figure 5B); it is presented as the entire transverse slice in Figure 5C. Similarly, transverse slices from **CyZW-274**-injected mice showed negligible signal (Figure S16). When the PA intensity represented by the brighter region (pseudo color) is compared across the skin, it is quite clear that localization of the probe signal is significantly higher in the younger mouse, indicating the presence of a higher amount of elastin. We found that the across all the slices, the average PA signal intensity from skin was ~1.8 times higher in the young mouse than in the older mouse, which is in good correlation with the fluorescence imaging data (Figure 5D). An essential element of the dermal connective tissue, elastin fibers, decreases with age as a result of reduced synthesis and increased degradation, resulting in skin sagging and reduced skin elasticity. This result indicates that **ElaNIR** is capable of showing differences between young and old mice and the underlying change in elastin that comes with aging.[31]

In summary, we have discovered **ElaNIR** as a NIR bioimaging probe suitable for *in vitro*, *ex vivo*, and *in vivo* imaging of elastin structures. **ElaNIR** offers a simple and convenient tool for fluorescence imaging of elastic structures, which will be valuable for understanding the function of elastin.

EXPERIMENTAL PROCEDURES

All procedures for animal experiments were approved by the Institutional Animal Care and Use Committee at the Agency for Science, Technology, and Research (A*STAR) of Singapore. Full experimental procedures are provided in the Supplemental Information.

SUPPLEMENTAL INFORMATION

Supplemental Information includes Supplemental Experimental Procedures, 20 figures, and 6 tables and can be found with this article online at https://doi.org/10.1016/j.chempr.2018.02.016.

ACKNOWLEDGMENTS

We gratefully acknowledge intramural funding from the A*STAR (Agency for Science, Technology, and Research of Singapore) Biomedical Research Council and

from National Medical Research Council grant NMRC/TCR/016-NNI/2016. We would like to thank the SBIC-Bruker Preclinical Imaging Centre, Bruker Singapore (http://www.pci-lab.com/), SBIC-iThera Medical Imaging Centre, and SBIC-Nikon Imaging Centre for their state-of-the-art imaging equipment. We are also very grateful for the help of Dr. Jun-Young Kim, Hui Shan Cheng, Anandh Kumar Raju, Lim Hann Qian, and Tay Hui Chen.

AUTHOR CONTRIBUTIONS

D.S., C.L.T., and Y.-T.C. conceived the project. D.S. synthesized the **CyZW** library and conducted photophysical characterization and analysis. C.L.T., S.-J.P., J.-J.K., and A.S. performed animal imaging experiments. R.B., U.S.D., and M.O. performed the photoacoustic imaging. M.P., F.L., and M.M. performed the 3D ball-tissue imaging. S.S.K. and M.A.B. performed the *in vivo* mouse pharmacokinetic study. All authors participated in writing the manuscript.

DECLARATION OF INTERESTS

The authors declare no competing interests.

Received: May 8, 2017
Revised: September 28, 2017
Accepted: February 16, 2018
Published: March 29, 2018

REFERENCES AND NOTES

1. Patel, A., Fine, B., Sandig, M., and Mequanint, K. (2006). Elastin biosynthesis: the missing link in tissue-engineered blood vessels. Cardiovasc. Res. *71*, 40–49.

2. Wirtschafter, Z.T., Cleary, E.G., Jackson, D.S., and Sandberg, L.B. (1967). Histological changes during the development of the bovine nuchal ligament. J. Cell Biol. *33*, 481–488.

3. Cleary, E.G., Sandberg, L.B., and Jackson, D.S. (1967). The changes in chemical composition during development of the bovine nuchal ligament. J. Cell Biol. *33*, 469–479.

4. Ricard, C., Vial, J.C., Douady, J., and van der Sanden, B. (2007). In vivo imaging of elastic fibers using sulforhodamine B. J. Biomed. Opt. *12*, 064017.

5. Biela, E., Galas, J., Lee, B., Johnson, G.L., Darzynkiewicz, Z., and Dobrucki, J.W. (2013). Col-F, a fluorescent probe for ex vivo confocal imaging of collagen and elastin in animal tissues. Cytometry A *83*, 533–539.

6. Shen, Z., Lu, Z., Chhatbar, P.Y., O'Herron, P., and Kara, P. (2012). An artery-specific fluorescent dye for studying neurovascular coupling. Nat. Methods *9*, 273–276.

7. Fabian, J., Nakazumi, H., and Matsuoka, M. (1992). Near-infrared absorbing dyes. Chem. Rev. *92*, 1197–1226.

8. Sevick-Muraca, E.M., Houston, J.P., and Gurfinkel, M. (2002). Fluorescence-enhanced, near infrared diagnostic imaging with contrast agents. Curr. Opin. Chem. Biol. *6*, 642–650.

9. Frangioni, J.V. (2003). In vivo near-infrared fluorescence imaging. Curr. Opin. Chem. Biol. *7*, 626–634.

10. Choi, H.S., Nasr, K., Alyabyev, S., Feith, D., Lee, J.H., Kim, S.H., Ashitate, Y., Hyun, H., Patonay, G., Strekowski, L., et al. (2011). Synthesis and in vivo fate of zwitterionic near-infrared fluorophores. Angew. Chem. Int. Ed. *50*, 6258–6263.

11. Choi, H.S., Gibbs, S.L., Lee, J.H., Kim, S.H., Ashitate, Y., Liu, F., Hyun, H., Park, G., Xie, Y., Bae, S., et al. (2013). Targeted zwitterionic near-infrared fluorophores for improved optical imaging. Nat. Biotechnol. *31*, 148–153.

12. Kim, S.H., Lee, J.H., Hyun, H., Ashitate, Y., Park, G., Robichaud, K., Lunsford, E., Lee, S.J., Khang, G., and Choi, H.S. (2013). Near-infrared fluorescence imaging for noninvasive trafficking of scaffold degradation. Sci. Rep. *3*, 1198.

13. Teoh, C.L., Su, D., Sahu, S., Yun, S.W., Drummond, E., Prelli, F., Lim, S., Cho, S., Ham, S., Wisniewski, T., and Chang, Y.T. (2015). Chemical fluorescent probe for detection of abeta oligomers. J. Am. Chem. Soc. *137*, 13503–13509.

14. Vendrell, M., Zhai, D., Er, J.C., and Chang, Y.T. (2012). Combinatorial strategies in fluorescent probe development. Chem. Rev. *112*, 4391–4420.

15. Kang, N.Y., Ha, H.H., Yun, S.W., Yu, Y.H., and Chang, Y.T. (2011). Diversity-driven chemical probe development for biomolecules: beyond hypothesis-driven approach. Chem. Soc. Rev. *40*, 3613–3626.

16. Lee, J.S., Vendrell, M., and Chang, Y.T. (2011). Diversity-oriented optical imaging probe development. Curr. Opin. Chem. Biol. *15*, 760–767.

17. Vendrell, M., Lee, J.S., and Chang, Y.T. (2010). Diversity-oriented fluorescence library approaches for probe discovery and development. Curr. Opin. Chem. Biol. *14*, 383–389.

18. Lee, J.S., Kim, Y.K., Vendrell, M., and Chang, Y.T. (2009). Diversity-oriented fluorescence library approach for the discovery of sensors and probes. Mol. Biosyst. *5*, 411–421.

19. Samanta, A., Vendrell, M., Das, R., and Chang, Y.T. (2010). Development of photostable near-infrared cyanine dyes. Chem. Commun. (Camb.) *46*, 7406–7408.

20. Ornelas, C., Lodescar, R., Durandin, A., Canary, J.W., Pennell, R., Liebes, L.F., and Weck, M. (2011). Combining aminocyanine dyes with polyamide dendrons: a promising strategy for imaging in the near-infrared region. Chemistry *17*, 3619–3629.

21. Wolinsky, H., and Glagov, S. (1967). A lamellar unit of aortic medial structure and function in mammals. Circ. Res. *20*, 99–111.

22. O'Connell, M.K., Murthy, S., Phan, S., Xu, C., Buchanan, J., Spilker, R., Dalman, R.L., Zarins, C.K., Denk, W., and Taylor, C.A. (2008). The three-dimensional micro- and nanostructure of the aortic medial lamellar unit measured using 3D confocal and electron microscopy imaging. Matrix Biol. *27*, 171–181.

23. Muiznieks, L.D., Weiss, A.S., and Keeley, F.W. (2010). Structural disorder and dynamics of elastin. Biochem. Cell Biol. *88*, 239–250.

24. Reichheld, S.E., Muiznieks, L.D., Stahl, R., Simonetti, K., Sharpe, S., and Keeley, F.W. (2014). Conformational transitions in the crosslinking domains of elastin. J. Biol. Chem. *289*, 10057–10068.

25. Hernandez, S.E., Rodriguez, V.D., Perez, J., Martin, F.A., Castellano, M.A., and Gonzalez-Mora, J.L. (2009). Diffuse reflectance spectroscopy characterization of hemoglobin and intralipid solutions: in vitro measurements with continuous variation of absorption and scattering. J. Biomed. Opt. *14*, 034026.

26. Wang, L.V., and Hu, S. (2012). Photoacoustic tomography: in vivo imaging from organelles to organs. Science *335*, 1458–1462.

27. Wang, L.V. (2009). Multiscale photoacoustic microscopy and computed tomography. Nat. Photonics *3*, 503–509.

28. Yao, J., and Wang, L.V. (2013). Photoacoustic microscopy. Laser Photon. Rev. *7*, 758–778.

29. Ku, G., and Wang, L.V. (2005). Deeply penetrating photoacoustic tomography in biological tissues enhanced with an optical contrast agent. Opt. Lett. *30*, 507–509.

30. Ho, C.J., Balasundaram, G., Driessen, W., McLaren, R., Wong, C.L., Dinish, U.S., Attia, A.B., Ntziachristos, V., and Olivo, M. (2014). Multifunctional photosensitizer-based contrast agents for photoacoustic imaging. Sci. Rep. *4*, 5342.

31. Shapiro, S.D., Endicott, S.K., Province, M.A., Pierce, J.A., and Campbell, E.J. (1991). Marked longevity of human lung parenchymal elastic fibers deduced from prevalence of D-aspartate and nuclear-weapons related radiocarbon. J. Clin. Invest. *87*, 1828–1834.